Lemos, G.V.B.; Cunha, P.H.C.P.; Nunes, R.M.; Bergmann, L.; dos Santos, J.F.; Clarke, T.:

Residual stress and microstructural features of friction-stir-welded GL E36 shipbuilding steel

In: Materials Science and Technology (2017) Taylor & Francis

DOI: 10.1080/02670836.2017.1361148

Residual stress and microstructural features of friction-stir-welded GL E36 shipbuilding steel

LEMOS, G. V. B.[1, 2], CUNHA, P. H. C. P.[1]; NUNES, R. M. [2]; BERGMANN, L.[1]; DOS SANTOS, J. F.[1]; STROHAECKER, T.[2]

[1] *Helmholtz-Zentrum Geesthacht GmbH, Institute of Materials Research, Materials Mechanics, Solid State Joining Processes (WMP), Geesthacht, Germany*

[2] *Post-graduation Program in Mining, Metallurgical and Materials Engineering (PPGE3M), Federal University of Rio Grande do Sul (UFRGS), Porto Alegre, Brazil.*

Abstract

The purpose of the present study was to fulfil the knowledge gap concerning residual stresses assessment for shipbuilding steels processed by friction stir welding (FSW), specifically for the grade GL E36. Plates of 6-mm thickness were welded by a solid state process using two different welding speeds (1 mm/s and 3 mm/s) and keeping the tool rotational speed constant at 500 rpm. Therefore, the joints experienced different thermal cycles, resulting in variable metallurgical and mechanical features. The work reported herein also quantifies the heat input of FSW as a function of welding parameters. The surface residual stress analysis was performed through the X-ray diffraction (XRD) technique. In addition, microstructure and microhardness studies were performed to support the residual stress distributions. The results showed that different welded joints have a distinguishable residual stress distribution. Transverse residual stresses up to 98% of the yield strength were observed at the lower heat input condition (3 mm/s). Increasing the welding speed led to higher residual stress states and microhardness in the stir zone.

Keywords: Friction Stir Welding, Shipbuilding, Residual Stresses, X-ray diffraction, Microstructure

1. Introduction

In the shipping building industry, the presence of welding operations is inevitable. Consequently, a solid-state joining process having low heat input is a promising way of joining shipbuilding steels for defect-free welds. Therefore, friction stir welding (FSW),

[1] as a solid state welding process, has strong potential to overcome the existing challenges related to the application of steels as far as the cost effective tools are accessible. Friction stir welding (FSW) had success when applied to aluminum alloys, and this fact was a driving force of the stimulated exploration of its applicability to other materials, such as steel [2]. This welding method has expanded rapidly since its development in 1991 and has found several applications in many industrial fields, including aerospace, automotive, railway and maritime [3]. The process applied to steel offers many advantages as low residual stresses and resulting distortion, no filler metal required, possibility to join dissimilar alloys, no risk of hydrogen-induced cracking, the absence of solidification cracking, porosity or cast microstructure [4-7] The FSW process is being actively developed for various shipbuilding activities and likewise critical applications, such as welding of high-strength pipelines. Furthermore, the distortion has also attracted interest from shipyards [8].

Unsurprisingly, residual stress-free welds do not exist. In general, for both fusion and solid state welding processes, due to the thermal cycles experienced, phase transformations and/or non-uniform deformation generate residual stress states that cannot be excluded and should be mitigated. Thus, even FSW, which can be a fast joining process below the material's melting point, will result in considerable residual stress states [9]. Structural failure is often related to the combination of two effects: residual stress and applied stress. These stress states can be detrimental or beneficial, depending upon their nature. Tensile residual stress in welded joints can lead to higher mean combined applied stress and then negatively affect the fatigue life, whereas compressive residual stress decreases the mean combined applied stresses and leads to an improvement in fatigue life [10]. Friction stir welding is a well-known process for achieving low distortion and residual stress states in welded components [4-7]. However, the rapid thermal cycle in localized areas during the joining process results in thermal expansion and contraction, which cause residual stress distributions in a welded component [11]. Hence, there is no doubt that large residual stress distributions presented in friction stir welding must be evaluated and understood to ensure the integrity of the welded joint.

Residual stresses in friction stir weldments have been evaluated several times [12-18]. However, most cases are related to Al alloys. In many studies, longitudinal residual stress distributions [e.g., parallel to the joint] in FSW joints show an "M" tendency with larger tensile stress values than in the transverse stress direction [13, 15, 18, 19, 20]. In

the direction of the base material, the residual stress states decrease and are balanced by compressive stresses. It is possible to estimate fatigue properties by residual stress states using the Goodman approach [19, 21].

Evaluation of the top surface welds characteristics is important because that region is normally exposed to the environment and its integrity and quality are related to surface phenomena, such as corrosion, wear, fatigue and residual stresses. Furthermore, initiation of fatigue cracks is directly linked with the surface of welded components as well as residual stresses. Thus, the present study evaluates the residual stress and microstructural features after friction stir welding applied to GL E36 shipbuilding steel.

2. Experimental procedure

The base material used in this study was 6 mm thick GL E36 steel plates, and its chemical composition is shown in Table 1. The data were provided by the supplier's certificate.

Table 1. Chemical composition (%wt).

Grade	Fe	C	Mn	Si	P	S	Cr	Mo	V	Ti	Al	Nb
GL E36	Bal.	0.17	1.40	0.39	0.013	0.001	0.060	0.006	0.004	0.003	0.027	0.025

Prior to the welding process, the top and adjoining surfaces of the plates were grinded to remove the oxide layer from its surface using a portable grinding tool with an 80 mesh sandpaper wheel. The samples were then immediately cleaned with ethanol before the welding step. This preparation of the surfaces procedure was an important step to improve the weld surface quality at the first joining trials. However, the process may have affected the residual stress states.

FSW was conducted on a vertical milling machine fitted with servomotors and automated control systems. A threaded polycrystalline cubic boron nitride (pcBN) tool from MegaStir™ with W-Re binder was used, commercially supplied with the specification Q70. The tool had a shoulder dimension of 25 mm and probe length of 6 mm. The direction of the tool rotation was counterclockwise, and the left side of the weld bead was called the retreating side (RS), whereas the right side was the advancing side (AS). The welding direction was parallel to the rolling process. To obtain the

welds, the tool was tilted 1.5° forward from the vertical, and an argon atmosphere was utilized to minimize the surface oxidation during FSW.

To observe the top surface and cross-section microstructures of the welded joints, a Nital solution 3% was prepared. The standard metallographic preparation using abrasive papers and diamond polishing solution was adopted.

The microhardness profiles across the welded beam on the top surface were measured by a Zwick Roell Indentec ZHV 2 system using HV0.3 and 0.4 mm of distance between indentations. Additionally, microhardness mapping measurements were performed using a hardness scanner model UT 100 supplied by BAQ. To build the maps, both measurements between the lines and columns were also 0.4 mm.

The original size of the welded joint was 280 x 210 x 6 mm, but the samples used for surface residual stresses had dimensions of 80 x 210 x 6 mm, with the weld centerline located in the center of the 210 mm dimension. The samples were cut from the original welded plate by electrical discharge machining (EDM) and any change in residual stress states could be excluded. X-ray diffraction residual stress measurements of the FSW shipbuilding steel was performed with a diffractometer model GE-Seifert-Charon-M (Figure 1) equipped with an X-ray tube of Cr-Kα radiation. XRD residual stress experiments were performed with the starting point at the base material in the retreating side (RS), passing by the weld centerline and then finishing at the base material in the advancing side (AS) in two conditions, named as-received and as-removed. A schematic sketch detailing the cutting plans and residual stress measurement positions can be seen in Figure 2. The diffracted beam slit had an aperture of 2 mm and a 20º linear detector GE-Meteor-1D. Residual stress evaluation used the conventional $\sin^2 \psi$ method with Bragg-Brentano Geometry. The {220}-lattice planes at $2\theta = 128.78°$ were chosen for the analysis. The measured range in 2θ was from 120° to 139° in steps of 0.1° with measurement times of 20 s. The slope of the linear regression through the measured data points gives the value of the residual stress. The standard deviation of the residual stress measurements stems from deviations of the X-ray diffraction line positions at 21 different angular positions (ψ-angles) to the calculated regression line. For the calculation of the residual stresses, elastic constants ½ s2 and –s1 were taken to be equal to 5.81E-6 MPa^{-1} and -s1 equal to 1.270-6 MPa^{-1}. The residual stress distributions were extensively examined for both the welded plates in two directions of measurements (longitudinal and transverse). In all, the total measured length was 80 mm. Because the size of the incident X-ray beam was 2 mm,

irradiated areas touched each other. An electrochemical polishing procedure was then performed using a solution of 80% H_2SO_4 and 20% H_3PO_4 acid and applying appropriate voltage (2 V) and current (1 A), and the residual stress distributions were measured again at a depth of 100 µm below the surface.

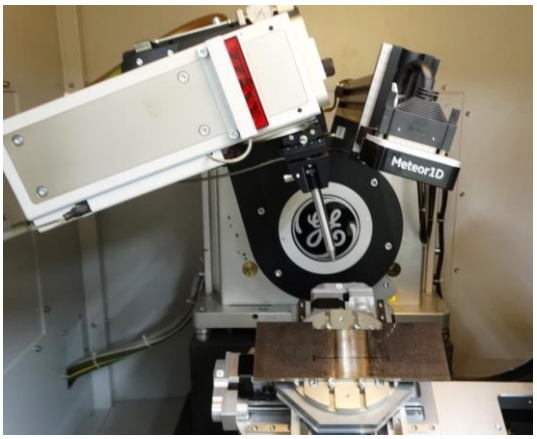

Figure 1. D*iffractometer* model GE-Seifert-Charon-M equipped with an X-ray tube of Cr-Kα radiation and Meteor 1D linear fast detector.

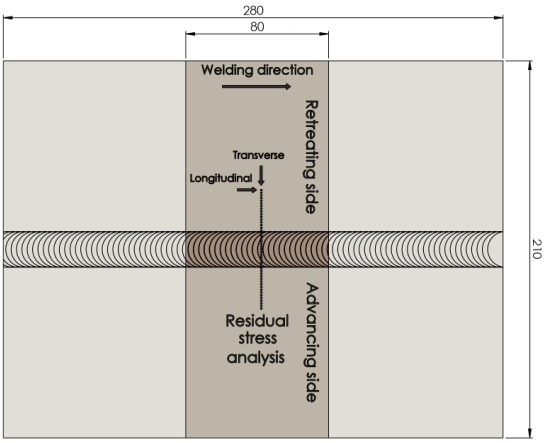

Figure 2. Schematic sketch of XRD residual stress positions in the welded plates.

3. Results and discussion

3.1 Welded joint top surface appearance

Two GL E36 shipbuilding steel plates were successfully welded by a friction stir process, reaching good aesthetic appearance. The welding speed (mm/s) was changed from 1 to 3 mm/s, the axial force was in the range between 40 and 50 kN and the rotational speed was constant. The weld top surface quality of the joints displayed homogeneous surface quality virtually without any flash, as illustrated in Figure 3; however, some signs of oxidation and marks were noted. Thus, electrochemical superficial layer removal was also employed in the present study to observe the effect of the final surface condition on the residual stress states. Flash is produced by material displacement from the face of friction stir welded components. Excessive flash may also result from improper tooling or parameter settings. Shoulder scrolling and reduced rotation rate are examples flash mitigation techniques [3]. The axial force has an important role in the quality of the weld. Very high pressures lead to overheating and thinning of the joint, whereas very low pressures lead to insufficient heating and voids

[6]. The weld face quality along the whole length was a good indicator that the forces involved during the process were stable, and the absence of flash after the welding process proved that the parameters used were suitable to maintain the stirred material within the joint.

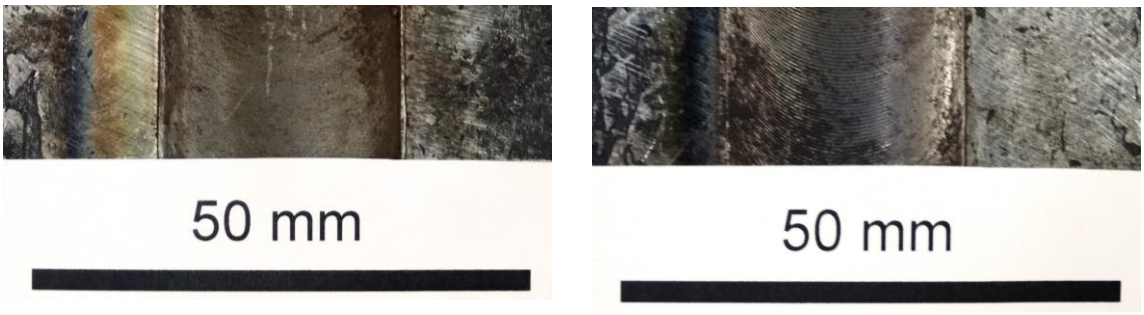

Figure 3. Surface initial conditions residual stress analysis a) 1 mm/s, b) 3 mm/s.

3.2 Heat input

One of the major FSW process advantages is that it has a relatively low heat input when compared with arc welding processes. Lower heat input in FSW is recognized with improved mechanical properties as well as decreased distortion and residual stresses [22]. Thus, depending on the FSW parameters set, the final heat input achieved and microhardness profiles of the welded joints may be altered. The heat input can be quantitatively calculated using the following equations [22].

$HI = \frac{P}{v}$	$P = \frac{(2\pi)\Omega T}{60}$

where P is power in kW, Ω is the rotational speed in rev/min, T the recorded spindle torque of the FSW machine in N.m, HI is the heat input in J/mm and v is the welding speed in mm/min. Finally, values for the heat input are given in *Table 2* according the welding parameters, from the highest to the lowest HI and named as 1 mm/s and 3 mm/s, respectively.

Table 2. Heat input as a function of the tool rotational speed and torque.

Welded joint	**Welding speed, mm/s**	**Rotational speed, rpm**	**Axial force, kN**	**Torque, N.m**	**Heat Input, kJ/mm**
1 mm/s	1	500	40	68	3.56

3 mm/s	3	500	55	92	1.61

As the welding speed increased, in general, less heat was applied because of the rapid movement of the FSW tool, thereby reducing the amount of friction heat [15]. Another explanation for this is that this correlation between the residual stress and welding speed would provide less time at elevated temperature for residual stress to relax [18]. Moreover, the higher the heat input is, the lower cooling rate. Therefore, residual stress states may be affected by these welding temperature characteristics.

3.3 Metallographic and microhardness assessment

The metallographic observations on the surface of the FSW joints are shown in Figure 4, Figure 6, Figure 8 and Figure 10, according to conditions 1 mm/s and 3 mm/s. The welded joint was divided along the traverse direction into five regions, identified as “a”, “b”, “c”, “d” and “e”, allowing a verification of each weld metallographic feature. These regions were used for the colored microhardness map (Figure 5 and Figure 9), microstructure analysis (Figure 6 and Figure 10) and microhardness profiles (Figure 7 and Figure 11). The asymmetric characteristics of the FSW process between the advancing and retreating sides [23] was caused by the material flow and was reflected in color patterns observed in the HV maps and the macrographs.

The macrographs results provided the first evidence of a residual stress gradient along the weld face length due to the presence of different distributions and the balance of miscellaneous microstructures between the two assessed parameters.

The colored microhardness maps offer a better way to assess the microhardness than the single line profiles because they exhibit the overall behavior of this property. The colored maps showed that the joints processed at higher welding speed, i.e., with lower heat input, exhibited a lower amount of harder microstructure (mainly the regions “a” and “c”, which can be seen in Figure 9), regardless of the higher cooling rates [24]. This contradiction is because the condition processed with 3 mm/s reached a lower peak temperature, resulting in smaller prior austenite grain size and leading to a higher tendency of diffusional transformations [25]. The microstructures present in the red areas (“a”, “c” and “e”) of the maps presented a higher amount of harder phases, like martensite and bainite, than softer microstructures, like ferrite, with different

morphologies. In contrast, the opposite balance was found within the green areas ("b" and "d") of the maps.

The microhardness profiles increased from the base material until the stirred zone due the gradual microstructure modification and/or transformation of the original microstructure (Figure 7 and Figure 11). The profiles demonstrated the overmatching features of the joints. The literature reports [6] that carbon steel alloys processed by FSW achieve an overmatching state; however, if the base material former microstructure is composed of martensite, then an undermatching joint will be produced [26]. The values measured within the stirred zone ranged from 300 HV to 440 HV. The single line HV profiles for the condition 3 mm/s presented a lower scatter among its measurements and a higher homogeneity along the whole weld face length. These values belong to the joint surface and vary though the weld thickness due to the different cooling comportments between the plate upper side and its inferior side, which was in direct contact with the backing bar located in the table of the welding machine.

Figure 4. Macrostructure ~~on~~ of the top surface of the condition 1 mm/s. AS stands for advancing side and RS for retreating side.

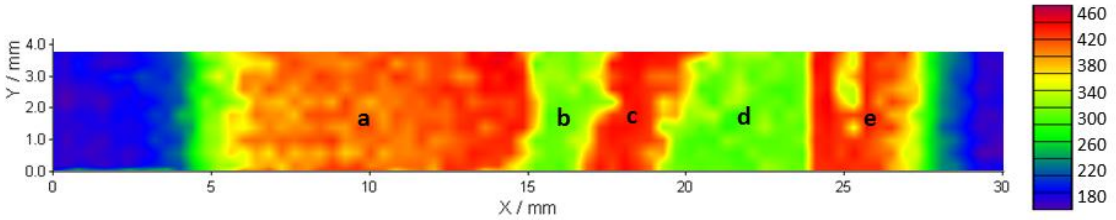

Figure 5. Colored top surface microhardness map (1 mm/s).

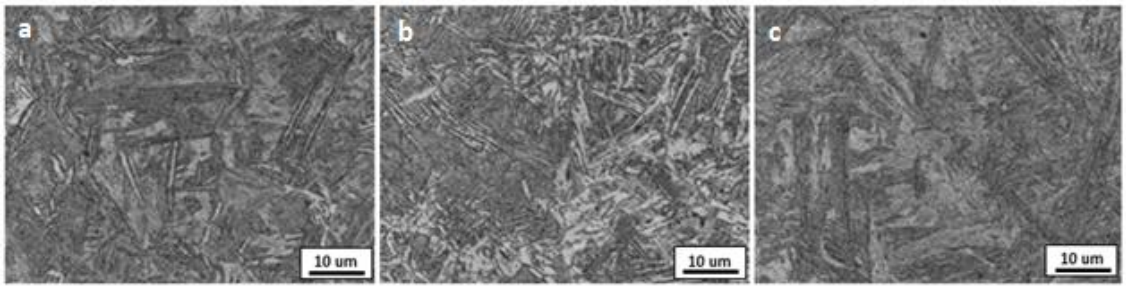

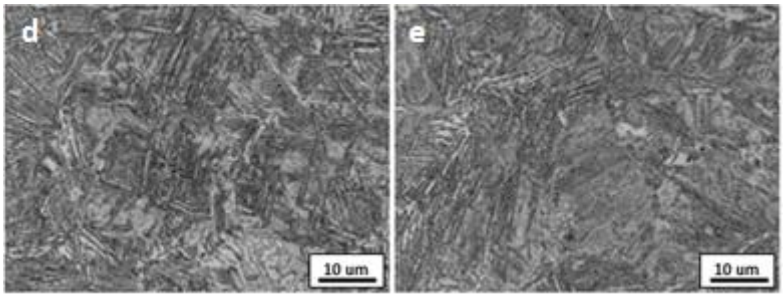

Figure 6. Microstructure on the top surface of the selected regions (1 mm/s).

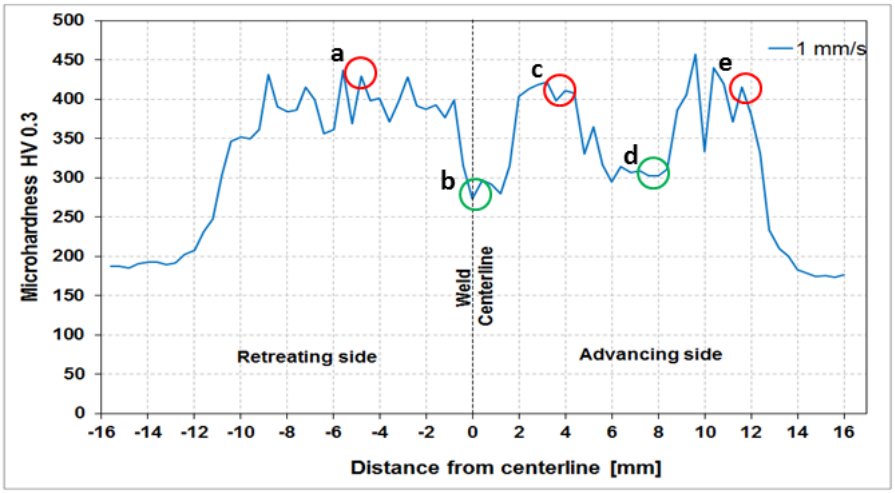

Figure 7. Middle HV profiles (1 mm/s).

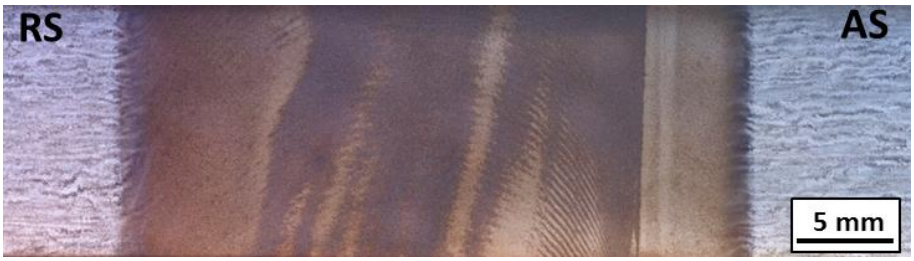

Figure 8. Macrostructure on the top surface of the condition 3 mm/s.

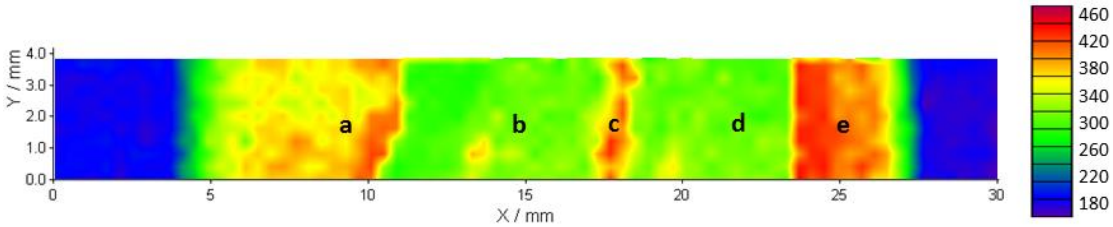

Figure 9. Colored top surface microhardness map (3 mm/s).

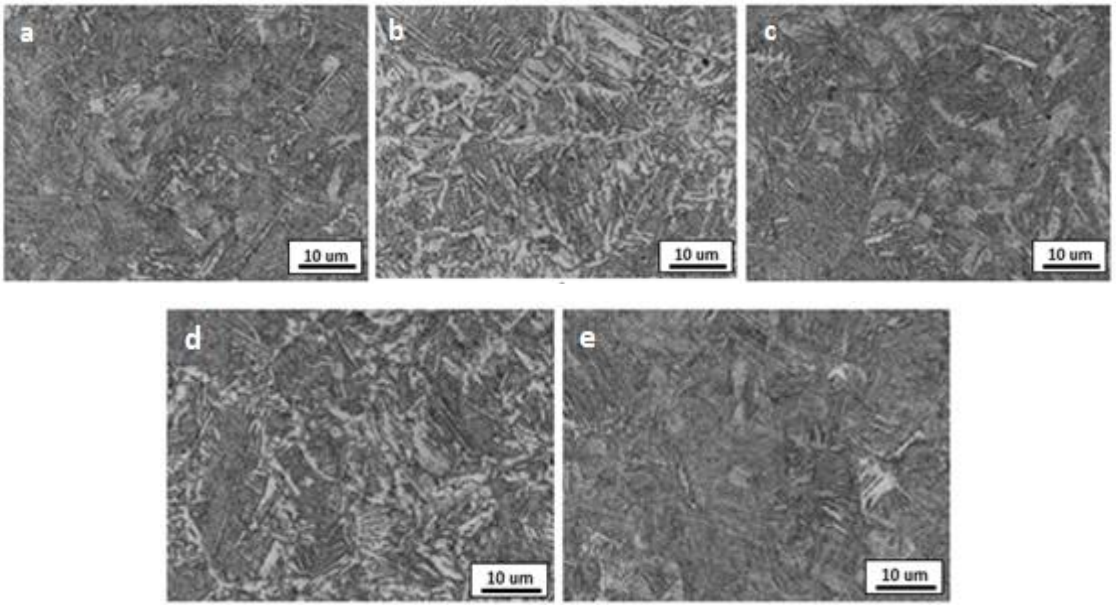

Figure 10. Microstructure on the top surface of the selected regions (3 mm/s).

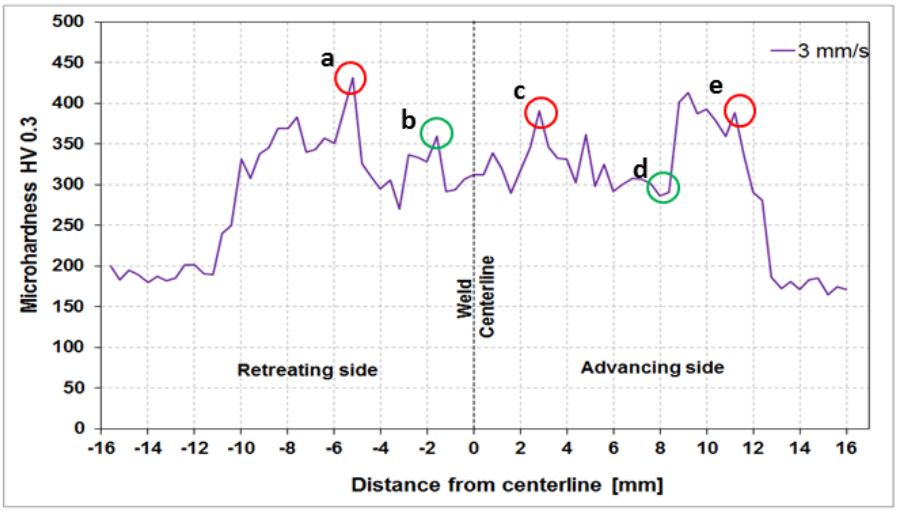

Figure 11. Microhardness HV profiles (3 mm/s).

The macrostructure for the cross-section of the FSW joint is presented in Figure 12a. Moving from the base material in the direction of the joint, the microstructure is firstly perlite and ferrite (Figure 12b), changes to degenerated perlite (Figure 12c) due to the solid state process, then to a spheroidized microstructure (Figure 12d) and finally to a complex mixed microstructure consisting mainly of ferrite, martensite and bainite within the stirred zone (Figure 3e).

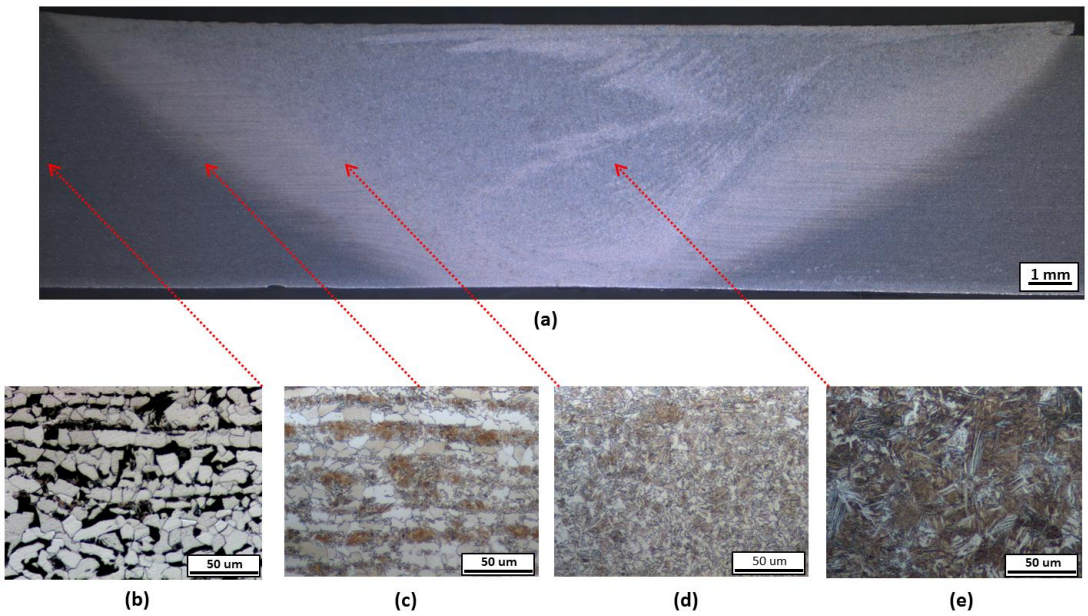

Figure 12. (a) Macrograph from the condition 3 mm/s and its microstructure gradient development (b)-(e).

Detailing the complex microstructure found in the stir zone for both joints, Figure 13 displays examples of microstructures at the weld centerline. And these images were classified using the nomenclature from the "Compendium of weld metal microstructures and properties" from TWI [27]. The code PF stands for intergranular polygonal ferrite, GF for grain boundary ferrite, AC for ferrite with aligned MAC (martensite, austenite or carbide), AF for acicular ferrite, B for bainite and M for martensite. Acicular ferrite (AF) is a highly desirable microstructure from the standpoint of toughness; however, ferrite distributed as grain boundary ferrite (GF) can adversely affect this property. Ferrite with aligned MAC (AC) is undesirable in an appreciable volume fraction when good toughness is being sought [28]. The acicular ferrite with fine interlocking microstructure significantly prevents the initiation and propagation of cracks [29].

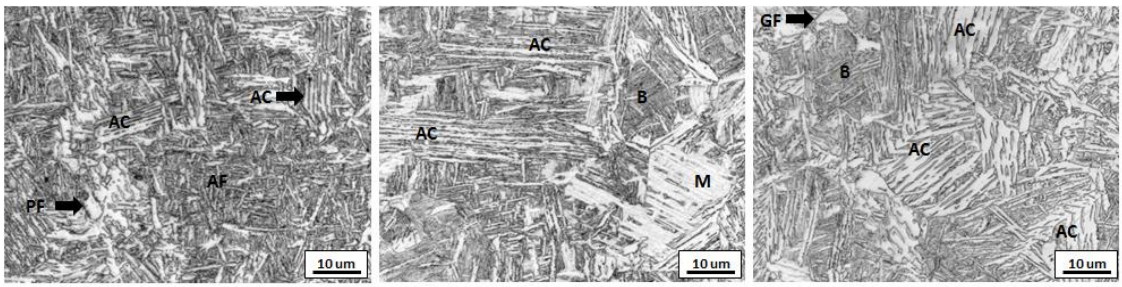

Figure 13. Examples of different morphologies from ferrite, bainite and martensite found in both of the experiments.

The microstructures identified at the stirred zone of the welds produced in the present study showed consistency with the evaluation of Reynolds et al. [30] when they applied the FSW process to grade DH36 of 6.4 mm in thickness. The results reported by Toumpis et al. [31] consisted of a comprehensive study using butts welded together at varying rotational and traverse speeds for DH36 shipbuilding grade steel of 6 mm in thickness. They stated that FSW generates a complex metallurgical system in which slow traverse speeds result in a very refined, ferrite-rich microstructure, intermediate traverse speeds produce predominantly acicular bainitic ferrites, and fast transverse speeds result in heterogeneous microstructures with distinct regions of acicular ferrite and acicular bainitic ferrite. In addition, the outcomes from the studies published by Barnes et al. [32] for grade HSLA-65 with 6.35 thicknesses indicated a similar microstructural behavior in accordance with the above studies and the present work.

3.4 Residual stress distributions

Longitudinal and transverse surface residual stress analysis in the condition as-welded (1 mm/s and 3 mm/s) for friction stir welded GL E36 plates is shown in Figure 14 and Figure 16. For the condition as-welded with a removed layer (100 μm), the residual stress states are displayed in Figure 15 and Figure 17. All measurements showed tensile stress regions that could be dangerous for fatigue properties. In contrast, the residual stress analysis also presented compressive stress regions that may slow fatigue crack growth~~l~~. Based on the macrostructure presented in Figure 12, the microstructural changes in the cross-section of the FSW joint influences the residual stress states presented in Figure 15 and Figure 17. There are also microstructural alterations in the top surface microstructure of friction stir weldments that can affect and explain the final residual stress distributions.

As can be observed in Figure 14, the longitudinal stress values increased with higher welding speed. On other hand, longitudinal residual stresses decreased for higher heat input, showing a good agreement with the literature [18]. Moreover, the residual stress profile across the welded joint displays an “M” trend with varied degrees of intensity, as previously reported [13, 15, 18, 19, 20]. In the welded centerline (stir

zone), the residual presents significant differences depending on the welding parameters. The condition 1 mm/s presents near zero residual stress behavior in the stir zone, and up to 15 mm from the weld centerline the residual stresses have the same tendency. The condition 3 mm/s presents a tensile residual stress behavior with residual stress values of approximately 100 MPa and, considering the weld centerline, it is obvious that the condition 3 mm/s has detrimental behavior in comparison with 1 mm/s due to the surface tensile residual stresses. In the retreating side (18 mm position) both welding parameters reached residual stress tensile peaks with values of approximately 300 MPa. On other side (advancing side), this behavior pattern occurs only for the condition 3 mm/s.

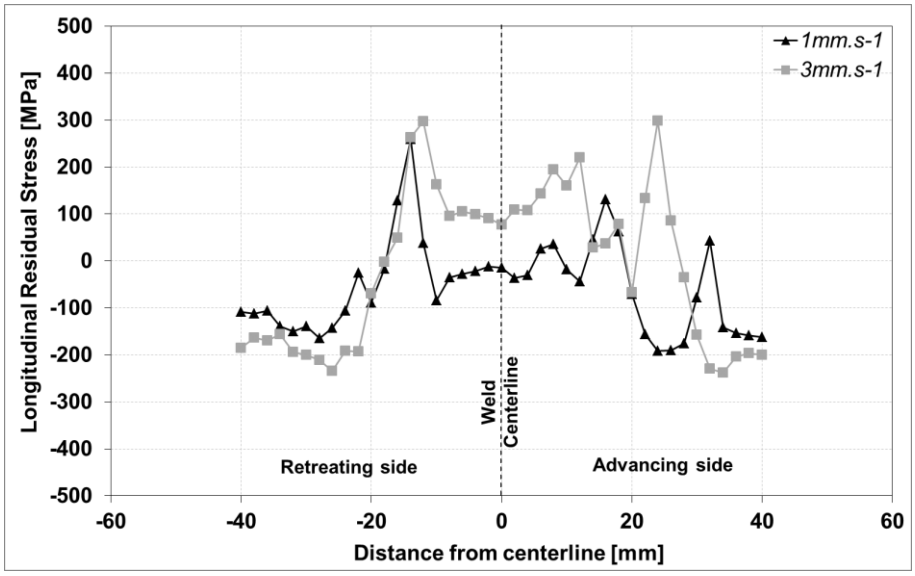

Figure 14. Longitudinal residual stress states measured by XRD from the top surface of each FSW plate in the condition as-welded.

The surface residual stress distributions along the plates notably changed after 100 μm of the electrochemical layer was removed and corrected by means of adaptation of Moore and Evans calculation method applied for plates [33]. Figure 15 shows a significant residual stress difference (200 MPa) in the stir zone for the welding parameters used. At the retreating side at distances up to 18 mm from the welding centerline, the residual stress states have tensile and compressive behavior depending on the welding parameters evaluated. Moreover, at distances greater than 20 mm from the weld center, the residual stresses present behavior and similar levels for both conditions

(1 mm/s and 3 mm/s). On the advancing side, the residual stress has the same trend, with the sample 1 mm/s reaching a tensile peak (197 MPa) at the 16 mm position.

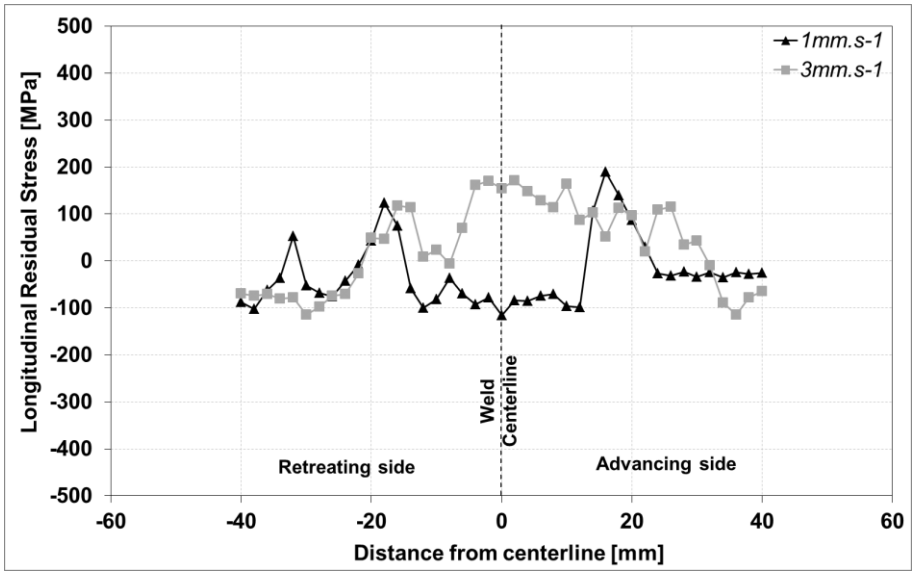

Figure 15. Longitudinal residual stress states measured by XRD from the top surface of each FSW plate in the condition as-welded with a removed layer.

The transverse stresses on the welded joint also increased with higher welding speed, as seen in Figure 16. As the heat input increased, the transverse stress values decreased [18]. The heterogeneity of the residual stress states is greater than the longitudinal stress results, as well as the asymmetry between the retreating and advancing side. The transverse stress distributions at the weld centerline are tensile for 1 mm/s (400 MPa) and 3 mm/s (198 MPa). The tensile stress peak (431 MPa) occurred in the advancing side at the same position (24 mm distance) as the removed layer results. This higher tensile stress value is 98% of the GL E36 yield strength (Ys), which is very dangerous in terms of fatigue life. Furthermore, the stress was found in a region that may have come from the cleaning procedures right before welding. If this welded joint is subjected to a high external load, a dangerous situation may be caused due to residual stresses close to the plastic deformation region; therefore, premature fracture could occur.

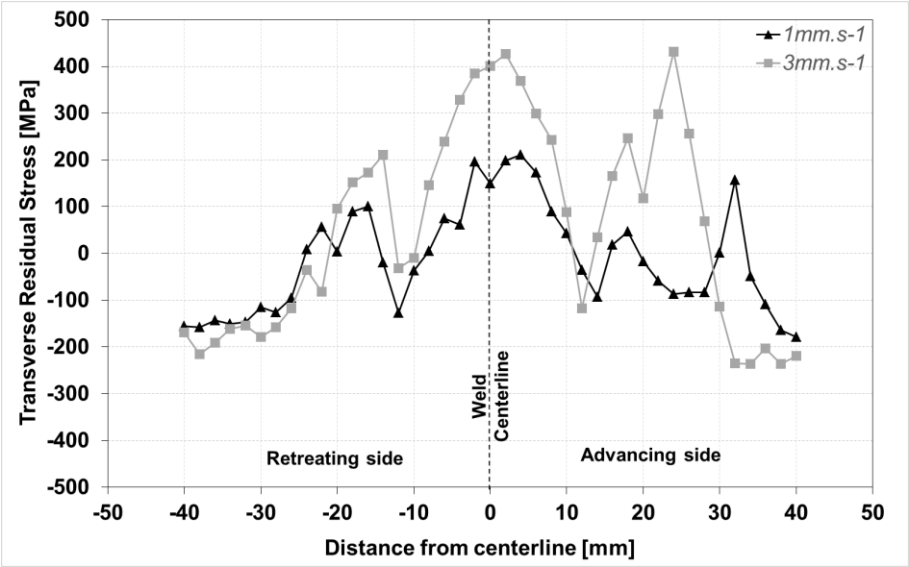

Figure 16. Transverse residual stress states measured by XRD from the top surface of each FSW plate in the condition as-welded.

The transverse residual stress distributions were also altered after removing the electrochemical layer. The stress values at the weld centerline (and consequently in the SZ) were moved down to a depth of 100 µm below the surface. The residual stress peak located at 26 mm for the condition as-welded was not strong in the removed layer condition. This value is related to the weld top surface characteristics. As with all of the residual stress results presented in this work, the condition 3 mm/s reached higher stress values in the stir zone. Figure 17 shows the highest residual stress difference (340 MPa) for the samples analyzed at the weld centerline.

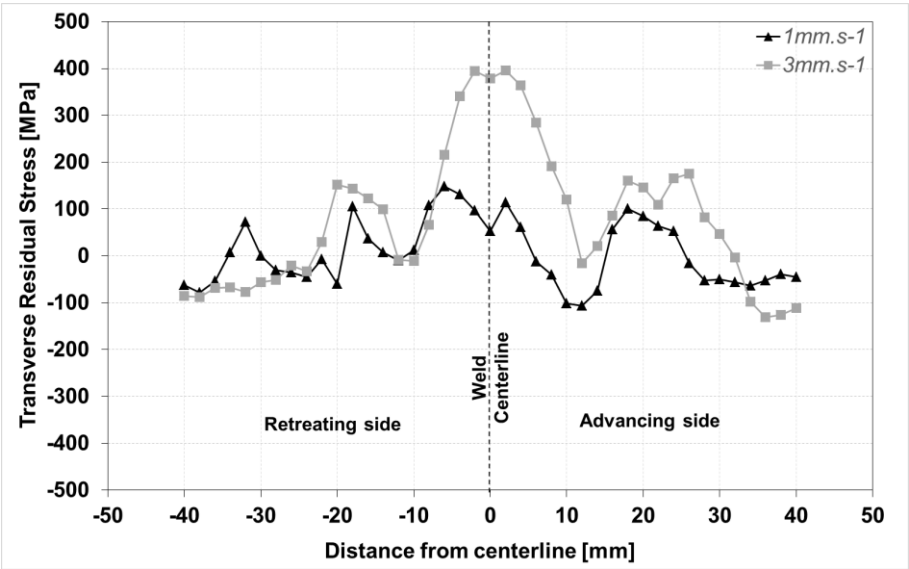

Figure 17. Transverse residual stress states measured by XRD from the top surface of each FSW plate in the condition as-welded with a removed layer.

5. Conclusions

Two FSW GL E36 shipbuilding steels were analyzed in the present study. XRD residual stress measurements were performed in the conditions as-welded and as-welded with a removed layer. The findings of the current investigation can be summarized as follows:

* The distribution and magnitude of the residual stress are closely connected to the microstructural changes present in the cross-section of the welds and in the top surface features. An increase in the welding speed increased the residual stress states and microhardness in the stir zone. A microstructural gradient was found within the stirred zone mainly consisting of ferrite, martensite and bainite with different levels of refinement and morphologies.

* Considerable tensile residual stress was observed in the condition as-welded for the welding parameter 3 mm/s, which indicates that this joint could not be used in real life without a machining step. Residual stress analysis after electrochemically removing a layer revealed changes in the initial residual stress states due to the microstructural gradient in the cross-section of the joints.

6. Acknowledgments

The authors of this work would like to thank CNPq (National Council for Scientific and Technological Development) through the Science Without Borders Program and CAPES (Brazil), as well as Helmholtz-Zentrum Geesthacht GmbH (Germany) for their support to execute this project.

7. References

1. THOMAS, WM; NICHOLAS, ED; NEEDHAM, JC; MURCH, MG; TEMPLE-SMITH, P; DAWES, CJ. Friction-Stir Butt Welding, GB Patent No. 9125978.8, International patent application No. PCT/GB92/02203, (1991)

2. H.K.D.H. Bhadeshia, T. DebRoy, Science and Technology of Welding and Joining, 14 (2009) 193-196.

3. B.T. Gibson, D.H. Lammlein, T.J. Prater, W.R. Longhurst, C.D. Cox, M.C. Ballun, K.J. Dharmaraj, G.E. Cook, A.M. Strauss, Journal of Manufacturing Processes, (2013).

4. G. Çam, International Materials Reviews, 56 (2011) 1-48.

5. R.S. Mishra, Z.Y. Ma, Materials Science and Engineering: R: Reports, 50 (2005) 1-78.

6. R. Nandan, T. Debroy, H. Bhadeshia, Progress in Materials Science, 53 (2008) 980-1023.

7. A. Pradeep, International Journal of Engineering Research and Development, 3 (2012) 75-91.

8. D. Lohwasser, Z. Chen, Friction Stir Welding - From Basics to Applications, Woodhead Publishing, 2009

9. Nilesh Kumar, Rajiv Mishra, John Baumann. Residual Stresses in Friction Stir Welding: A Volume in the Friction Stir Welding and Processing Book Series. 2013.

10. Suominen L, Khurshid M, Parantainen J. Residual stresses in welded components following post-weld treatment methods. Procedia Engineering. 2013 Dec 31;66:181-91.

11. Z. M. Hu, P. B. J. W. Brooks, Residual Stresses in Friction Stir Welding, in: 2004 ABAQUS Users' Conference (2004).

12. Richter-Trummer V, Suzano E, Beltrão M, Roos A, dos Santos JF, de Castro PM. Influence of the FSW clamping force on the final distortion and residual stress field. Materials Science and Engineering: A. 2012 Mar 15;538:81-8.

13. Steuwer A, Barnes SJ, Altenkirch J, Johnson R, Withers PJ. Friction Stir Welding of HSLA-65 Steel: Part II. The Influence of Weld Speed and Tool Material on the Residual Stress Distribution and Tool Wear. Metallurgical and Materials Transactions A. 2012 Jul 1;43(7):2356-65.

14. Terasaki T, Akiyama T. Mechanical behaviour of joints in FSW: Residual stress, inherent strain and heat input generated by friction stir welding. Welding in the World. 2003 Nov 1;47(11-12):24-31.

15. Peel M, Steuwer A, Preuss M, Withers PJ. Microstructure, mechanical properties and residual stresses as a function of welding speed in aluminium AA5083 friction stir welds. Acta materialia. 2003 Sep 15;51(16):4791-801

16. Reynolds AP, Tang W, Gnaupel-Herold T, Prask H. Structure, properties, and residual stress of 304L stainless steel friction stir welds. Scripta Materialia. 2003 May 31;48(9):1289-94

17. Staron P, Kocak M, Williams S, Wescott A. Residual stress in friction stir-welded Al sheets. Physica B: Condensed Matter. 2004 Jul 15;350(1):E491-3.

18. Brewer LN, Bennett MS, Baker BW, Payzant EA, Sochalski-Kolbus LM. Characterization of residual stress as a function of friction stir welding parameters in oxide dispersion strengthened (ODS) steel MA956. Materials Science and Engineering: A. 2015 Oct 28;647:313-21

19. Khandkar MZ, Khan JA, Reynolds AP, Sutton MA. Predicting residual thermal stresses in friction stir welded metals. Journal of Materials Processing Technology. 2006 May 25;174(1):195-203.

20. Buffa G, Fratini L, Pasta S. Residual stresses in friction stir welding: numerical simulation and experimental verification. Ininvited paper at ICRS-8 8th International Conference on Residual Stresses. Colorado, USA 2008 Aug

21. Lemmen, H.J.K., Alderliesten, R.C., Benedictus, R. (2010), Fatigue initiation behaviour throughout friction stir welded joints in AA2024-T3, International Journal of Fatigue 32(12):1928-1936

22. Lienert T, Stellwag Jr W, Lehman L, editors. Comparison of heat inputs: Friction stir welding vs. arc welding. AWS conference; 2002.

23. ARBEGAST, W.J. Hot Deformation of Aluminum Alloys. TMS, Warrendale, PA, USA, 2003, p. 313

24. L. Cui, H. Fujii, N. Tsuji, K. Nakata, K. Nogi, R. Ikeda, M. Matsushita, Isij Int, 47 (2007) 299-306

25. BHADESHIA, H. K. D. H., HONEYCOMBE, R. W. K. Steels: Microstructure and Properties. Butterworths-Heinemann, 2006

26. R. Ueji, H. Fujii, L. Cui, A. Nishioka, K. Kunishige, K. Nogi, Materials Science and Engineering: A, 423 (2006) 324-330.

27. T.W. Institute, International Institute of Welding, Abington, 1985

28. G.E. Linnert, FUNDAMENTALS WELDING METALLURGY, AWS, 1994.

29. M. Fattahi, N. Nabhani, M. Hosseini, N. Arabian, E. Rahimi, Micron, 45 (2013) 107-114.

30. A.P. Reynolds, W. Tang, M. Posada, J. Deloach, Science and Technology of Welding and Joining, 8 (2003) 455-460.

31. A. Toumpis, A. Galloway, S. Cater, N. McPherson, Materials & Design, 62 (2014) 64-75.

32. S.J. Barnes, A.R. Bhatti, A. Steuwer, R. Johnson, J. Altenkirch, P.J. Withers, Metallurgical and Materials Transactions A, 43 (2012) 2342-2355.

33. M.G. Moore and W.P. Evans, Trans. SAE, Vol.66, 1958, p. 340.